Published in final edited form as:
Colloids Surf B Biointerfaces. 1994 June 30; 2(5): 481–491. doi:10.1016/0927-7765(94)80056-1.

Human serum albumin adsorption onto octadecyldimethylsilyl–silica gradient surface

Yeong-Shang Lin[a] and **Vladimir Hlady**[b]

[a]Department of Materials Science and Engineering, University of Utah, Salt Lake City, UT 84112, USA

[b]Department of Bioengineering, University of Utah, Salt Lake City, UT 84112, USA

Abstract

The effects of long-range electrostatic repulsion and short-range hydrophobic attraction on human serum albumin adsorption were studied as a function of the surface density of octadecyldimethylsilyl chains (C18) on silica. A C18 surface density gradient was prepared on fused silica plates. The water contact angles increased smoothly from 12° to 105° in the 12.5 mm long gradient region. The maximal fractional surface coverage of the C18 chains was calculated to be 0.92. Fluorescein-5-isothiocyanate-labeled human serum albumin (FITC-HSA) adsorption from dilute buffer solution onto the C18 gradient surface was measured using spatially resolved total internal reflection fluorescence (TIRF) spectroscopy. FITC-HSA adsorbed progressively more onto the surfaces with higher hydrophobicity. When the fractional surface coverage of C18 chains was larger than 0.42 the adsorption saturation of FITC-HSA leveled off. The adsorption kinetics of FITC-HSA changed from a transport-limited process at moderate-to-high C18 surface coverages to an adsorption-limited process at lower C18 surface coverages. The kinetics of FITC-HSA adsorption, including the convective–diffusive transport of protein to the surface, were modeled as a simple binding process with a single forward and reverse rate. The apparent binding constant, derived from the initial forward and reverse binding rates, depended more strongly on the C18 surface coverage in 0.165 M buffer than in 0.025 M buffer.

Keywords

Human serum albumin adsorption; Kinetics; Surface density gradient; Total internal reflection fluorescence spectroscopy

Introduction

Observations that surfaces with a strongly bound albumin layer show a good, short-term biocompatibility have led to the postulation of the “albumin hypothesis of blood compatibility” [1]. This hypothesis was supported by experiments in which the alkylation of blood-contacting polymers with long linear alkyl chains, which are known to bind albumin

Correspondence to: Vladimir Hlady.

strongly, reduced thrombus formation at the blood/polymer interface [2,3]. Eberhart et al. [4] had proposed the covalent binding of 16- or 18-carbon alkyl chains to polymer surfaces as a way of improving the surface blood compatibility. Pitt et al. [5] studied human serum albumin (HSA) adsorption and desorption using alkyl-chain-derivatized polyurethane. By varying the chain length from 2 to 18 carbon atoms, Pitt et al. concluded that the total adsorbed amount increased with the chain length. The desorption rate decreased with the increasing alkyl chain length.

It is known that the binding affinity of albumin for the alkyl chains of the free fatty acids increases as the number of carbon atoms in the fatty acids increases from 6 to 18 [6]. The Scatchard analysis and other models applied to fatty acids binding to dissolved albumin indicated that HSA has six or seven strong fatty acid binding sites and several weak binding sites [6,7]. The interaction between surface-bound alkyl chains and albumin probably occurs via a similar hydrophobic mechanism. Such interactions could stabilize the albumin tertiary structure and thus preserve its inert character which, in turn, might block the surface-induced activation of coagulation and complement systems in the circulation.

Other hydrophobic surfaces may adsorb albumin in a different way from that of the surface with immobilized alkyl chains. Albumin adsorption on hydrophobic surfaces has been extensively studied in the past. Van Dulm and Norde [8] studied HSA adsorption on a hydrophobic siliconized glass surface. This surface showed a higher adsorption than the hydrophilic glass surface. Baszkin and Lyman [9] concluded that the adsorption value of HSA on hydrophobic surfaces, 0.25 μg cm^{-2}, corresponds to a surface monolayer of HSA. We have found a similar adsorption value in a fluorescence adsorption study of HSA using a hydrophobic, dimethylsilyl–silica surface [10].

One important use of surface-immobilized alkyl chains is in chromatography [11]. The conformation of surface-immobilized alkyl chains and the characterization of these chromatographic surfaces have been extensively studied using various methods, such as fluorescence [12,13], nuclear magnetic resonance spectroscopy [14,15], low-energy atom diffraction and grazing incidence X-ray diffraction [16]. According to the literature, in the case of a moderately high surface coverage of 18-carbon (C18) chains (approximately three C18 chains per 10 nm^2), the middle of the C18 chain is well ordered and less mobile, the chains may aggregate when water is added, and their mobility is impeded by steric interactions with other nearby C18 chains. For a C18 silica surface with a low surface coverage (approximately one C18 chain per 10 nm^2), the C18 chains are highly mobile when water is added. Often the chromatographic performance is only empirically correlated with the surface composition of the chromatographic stationary phase [17,18].

A self-assembled monolayer of octadecyltrichlorosilane (OTS) on silicon displays a high level of order and close monolayer packing [19,20]. Ellipsometric measurements of OTS monolayers on silicon also indicated a relatively dense OTS monolayer with a mean thickness equal to the length of fully extended alkane chains tilted from the surface normal by 15° or less [21]. Monolayers of alkylsilanes may be inherently more disordered than those of alkanethiols, where molecules have more freedom to establish along-range order [21].

In this paper we report on HSA adsorption onto C18 alkylated silica surfaces. We have prepared C18 silica surfaces covered with a complete C18 monolayer (a "self-assembled C18 film") and surfaces with a gradually varying surface coverage of C18 chains (a "C18 gradient surface"). The C18 gradient surface has a C18 monolayer on one end, pure silica on the other end and a surface density gradient of C18 alkyl chains in between these two ends. The concept of gradient surfaces was first introduced by Elwing et al. [22]. We have previously used surface gradients as a tool for characterizing protein surface adsorption [10,23]. The main advantage of using gradient surfaces is that, under the same experimental conditions, one can study how a particular surface parameter, i.e. wettability, charge etc., influences protein adsorption. Conversely, a protein with known interfacial characteristics may be used as a reporter molecule to study the distribution of the immobilized ligands in the surface gradient region.

The interaction between negatively charged surfaces partially covered with C18 alkyl chains and the dissolved albumin molecule presents an interesting problem from the point of view of the forces involved. The situation is schematically presented in Fig. 1. Because albumin at neutral pH carries an overall negative charge, the ensuing electrostatic interactions will cause a long-range repulsion between the protein and the negative surface. However, when a collision of albumin molecules with the surface-immobilized long alkyl chains occurs, it will result in a short-range hydrophobic interaction and the strong binding. The interplay between the short-range attractive forces and the long-range repulsive forces, which can be controlled by the ionic strength of the solution, is expected to determine how efficiently the electrostatic adsorption energy barrier will retard the adsorption.

In this study the adsorption kinetics of HSA labeled with fluorescein-5-isothiocyanate (FITC-HSA) onto C18 gradient surfaces were measured by spatially resolved total internal reflection fluorescence (TIRF) spectroscopy. The adsorption kinetics results were fitted with a simple adsorption model developed by Corsel et al. [24] and refined by Horsley [25]. The fitted parameters were the adsorption and desorption rates and the dependence of these parameters on the C18 surface coverage.

Materials and methods

Preparation of C18 gradient surface

Pyridine and dichloromethane (Merck), octadecyldimethylchlorosilane (ODS; Aldrich), and *p*-xylene (Fluka) were used as received. The self-assembled C18 surfaces were prepared with a dichloromethane–ODS–pyridine solution mixture (volume ratio 125:2:1) using procedures adapted from the literature [26–28]. After 4 h of reaction, silica plates (Esco; 2.5 × 7.5 cm^2) were rinsed twice with ethanol and acetone, then with deionized water, and were then dried with nitrogen gas.

The C18 gradient surface was prepared using the two-phase diffusion method [22]. Based on the results of the preparation of self-assembled C18 surfaces, the solvent chosen in the lower phase was dichloromethane (density $d = 1.325$ g cm^{-3}) instead of trichloroethylene ($d = 1.4$ g cm^{-3}) and the diffusion time was extended from 20 min to 4 h. After 4 h of reaction, the rinsing and drying procedures were identical to those used for the self-assembled C18

surfaces. The advancing and receding water contact angles (θ_{adv}, θ_{rec} respectively) of the C18 surfaces were measured by the dynamic Wilhelmy plate method as previously described [10].

HSA adsorption

Human serum albumin (HSA; ICN Immuno-Biologicals) was labeled with fluorescein-5-isothiocyanate (FITC; Aldrich). Free FITC has a major absorption peak at 494 nm and a minor absorption peak at 280 nm; the ratio of minor to major adsorption is 0.285. This ratio was assumed to be the same for HSA-bound FITC. The HSA extinction coefficient, $\varepsilon = 0.54$ ml mg^{-1} cm^{-1} at 280 nm, was used to determine the HSA concentration. The degree of labeling of FITC–HSA was 0.70. The FITC-HSA solution was diluted to 0.042 mg ml^{-1} (approximately 1/1000 of albumin blood concentration) using one of two buffers: 0.165 M ionic strength phosphate buffered saline (PBS; pH 7.4; 0.008 M Na_2HPO_4 + 0.001 62 M KH_2PO_4 + 0.14 M NaCl) or 0.025 M ionic strength PBS (pH 7.4; 0.008 M Na_2HPO_4 + 0.001 62 M KH_2PO_4).

The HSA adsorption was performed using the spatially-resolved TIRF apparatus [29]. A TIRF cell with two rectangular flow channels was used. Two parallel experiments could be performed using the identical C18 gradient surface. The two-flow-channel flow cell enabled an exact registration of the C18 surface coverage in parallel experiments. The HSA and pure PBS solutions were injected through the cell during the respective adsorption and desorption segments of the experiment. The flow rate was 1.0 ml min^{-1}. The experiment was started with an 11 min adsorption segment followed by an 11 min desorption segment. The Ar^+ ion laser (Lexel; model 92) was used for the excitation of the adsorbed FITC-HSA fluorescence. The laser beam (10 mW at 488 nm) was expanded to a diameter of 25 mm, collimated and passed through a rectangular mask (size 4×9 mm^2). Approximately 1 mW of the power totally reflected from an area of size 4×26 mm^2 inside the flow channel resulted in a power density of approximately 10 μW m^2. Under the conditions used in the experiments, the contribution from the FITC-HSA solution fluorescence to the observed fluorescence signal was negligible. The fluorescence intensity profile along the C18 gradient was recorded every second during the adsorption/desorption cycle using a charge-coupled device (CH220; Photometrics). Further experimental details of the spatially resolved TIRF adsorption technique can be found in Ref. 29.

The conversion of fluorescence intensity into the surface density of FITC-HSA

The FITC-HSA adsorption on to the fully hydrophobic end of the C18 gradient surface was assumed to be initially a transport-limited process. This assumption was supported by preliminary experiments where different concentrations of FITC-HSA solution were used and by the literature data [30]. In the case of the transport-limited adsorption, the initial rate of adsorption is limited by the availability of protein molecules at the adsorbing surface, which, in turn, is determined by the hydrodynamic parameters of the flow channel, protein diffusion coefficient and solution concentration of protein [29,31]. A factor for converting the fluorescence intensity of adsorbed FITC-HSA to the surface density of FITC-HSA was calculated from the Leveque equation:

$$dA/dt=[\Gamma(4/3)]^{-1}9^{-1/3}(6q/b^2wlD_{HSA})^{1/3}D_{HSA}c_{HSA} \quad (1)$$

where d*A*/d*t* is the flux of protein molecules to the surface, *q* is the experimental volumetric flow rate, *b* = 0.05 cm is the thickness of the TIRF flow cell, *w* = 0.4 cm is the width of the cell, *l* is the down-stream distance from the position where adsorption starts to appear, D_{HSA} = 6.7 × 10^{-7} cm^2 s^{-1} is the diffusion coefficient of HSA [29], c_{HSA} = 42 μg cm^{-3} is the FITC-HSA concentration used in this study and Γ is the gamma function: $(\Gamma(4/3))^{-1}9^{-1/3}$ = 0.539 14.

In order to identify the experimental rate of adsorption with the calculated protein flux to the surface, one also needs to assume that the rate of adsorption is not significantly diminished by the concurrent desorption process. In this study the desorption rates were calculated directly from the fluorescence intensities recorded during the desorption segment of the experiment. They are typically very low (see Table 1) and introduced a negligible error in the conversion of fluorescence into the adsorbed amount.

Modeling the FITC-HSA adsorption kinetics

The experimental FITC-HSA adsorption results were fitted into an adsorption model developed by Corsel et al, [24] and implemented as a numerical computer simulation by Horsley [25]. The adsorption rate (dΓ/d*t*) is expressed as

$$d\Gamma(t)/dt=k_{on} \times [\Gamma_{max}-\Gamma(t)] \times C(0,t)-k_{off} \times \Gamma(t) \quad (2)$$

where Γ(*t*) is the adsorbed mass of protein per unit surface at time *t*, Γ_{max} is the value of Γ at maximal surface coverage, and k_{on} and k_{off} are the intrinsic adsorption and desorption rate constants respectively. The model assumes that the adsorption rate is proportional to the free surface, (Γ_{max} − Γ(*t*)), and to the concentration of protein at the adsorbing surface, *C*(0,*t*).

The model defines the intrinsic rate constants, k_{on} and k_{off}, as the exponential functions of the surface protein concentration Γ:

$$k_{on}=k_1\exp(-\alpha\Gamma) \quad (3a)$$

$$k_{off}=k_{-1}\exp(\beta\Gamma) \quad (3b)$$

where k_1 and k_{-1} are the initial intrinsic adsorption and desorption rate constants, respectively, and α and β are so-called “cooperativity” constants. Cuypers et al. [32] have used these k_{on} and k_{off} empirical equations to model lateral protein interactions.

In the present study the k_{-1} values were determined by fitting the initial desorption segment of the experimental kinetics. In this case *C*(0,*t*)≈0 and

$$d\Gamma(t)/dt=-k_{off} \times \Gamma(t) \quad (4)$$

After the k_{-1} values were found, the fitting of the adsorption segment of the experiments was performed. The adsorption simulation program was written in Pascal to run on a Macintosh II computer [25]

Results

Wettability of C18-silica surface

The self-assembled C18 film on the silica surface displayed water contact angles θ_{adv} = 105°, θ_{rec} = 84° and $\Delta\theta = \theta_{adv} - \theta_{rec}$ = 21° respectively. By assuming that θ_{C18}= 112° [33] and θ_{silica} = 0°, the Cassie equation [34] was used to calculate the fraction of the surface covered with C18 chains, *f*:

$$\cos\,\theta_{adv} = f\,\cos\,112^{\circ} + (1-f)\,\times\,\cos\,0^{\circ} \quad (5)$$

At θ_{adv} = 105°, the fractional surface coverage of C18 was 0.92. The contact angle hysteresis, Δθ, also indicated that the self-assembled film of C18 alkyl chains was not defect free. It is possible that water penetrated into the incomplete coverage regions of the C18 layer, making θ_{rec} smaller than θ_{adv}.

The conditions used to prepare the self-assembled C18 film on the silica surface were also employed in the preparation of the C18 gradient surface on silica plates. The dynamic contact angles measured on the C18 gradient surface are shown as a function of the distance from the hydrophilic end of the plate in Fig. 2. The C18 end of the gradient surface had the same contact angles as the self-assembled C18 film. The contact angles of the hydrophilic silica end of the gradient surface were θ_{adv} = 12°, θ_{rec} = 0° and Δθ = 12°. Between these two ends was a 12.5 mm long C18 surface density gradient; its θ_{adv} and θ_{rec} values change smoothly along the gradient direction. The Δθ hysteresis in the region of the C18 surface density gradient was larger than at the C18 end, possibly due to the effect of the local packing of C18 chains. The less tightly packed C18 chains, especially the outer half of the C18 chains, will, upon the addition of water, result in a progressively smaller θ_{rec}.

The clean silica should have contact angles $\theta_{adv} = \theta_{rec}$ = 0°. The non-zero advancing contact angle was possibly an indication of a slight contamination of the silica surface. As will be seen below, this contamination had no effect on the FITC-HSA adsorption kinetics.

Kinetics of FITC-HSA adsorption

The pattern of FITC-HSA adsorption onto the C18 gradient from 0.165 M ionic strength PBS measured with the spatially resolved TIRF technique is shown in Fig. 3. The two markers indicate the regions of the gradient surface: hydrophilic silica, the C18 gradient region and the C18 surface, and correspond to the respective distances of 32.5 mm and 45.0 mm in Fig. 2. The FITC-HSA solution was injected through the flow cell from the silica end and passed out of the flow cell at the C18 end. There was no measurable increase in the fluorescence intensity at the silica end of the gradient surface, indicating that, at the concentrations used in this study, FITC-HSA did not adsorb to silica. It also showed that the contribution of solution FITC-HSA fluorescence to the overall fluorescence signal was negligible, i.e. that the fluorescence excited by the evanescent surface wave indeed

originated from the adsorbed protein only. The first increase in fluorescence was measured at the onset of the C18 gradient region, indicating that FITC-HSA adsorbed there. As the surface density of C18 chains increased, so did the level of FITC-HSA surface fluorescence. At the gradient positions $\theta_{adv} > 65°$ the steady state levels of fluorescence remained unchanged with further increase in the C18 surface density. The initial increase in fluorescence in the upper gradient region also remained unaffected by the C18 surface density, a feature that is expected for the transport-limited adsorption process. The desorption segment of the experiment resulted in a very slow and incomplete removal of adsorbed protein. The TIRF adsorption pattern obtained in the parallel experiment performed from 0.025 M ionic strength PBS (data not shown here) displayed features similar to those in Fig. 3.

Prior to the fitting of the experimental adsorption results to a model, the fluorescence intensity of adsorbed FITC-HSA was converted to surface density using the Leveque equation (Eq. (1)). As discussed earlier, the kinetics of FITC-HSA adsorption at the p1 position indicated in Fig. 2 (37.5 mm; $\theta_{adv} = 75°$) was assumed to be a purely transport-limited process. The flux of FITC-HSA to the surface was calculated to be $dA/dt = 1.27 \times 10^{-2}$ μg cm^{-2} s^{-1}. By comparing the dA/dt with the rate of fluorescence increase at the position p1, the conversion factor of 4.56×10^{-4} μg cm^{-2} per count of fluorescence intensity was calculated. All surface concentrations of FITC-HSA were calculated from the respective fluorescence intensities using the same conversion factor.

Two examples of the fit between the experimental adsorption kinetics and the simulated model kinetics are shown in Fig. 4. Only the first 5 min of the adsorption were selected for comparison with the model. The points shown in Fig. 4 were determined by the TIRF experiments at the middle of the gradient region (position p2 at 35.7 mm in Fig. 2; $\theta_{adv} = 54°$) for the FITC-HSA adsorption from 0.165 M and 0.025 M ionic strength PBS. The solid lines are simulated model results. Equally good fits were obtained for other experimental results measured at the other two positions of the C18 gradient: p1 and p3 ($\theta_{adv} = 50°$). The model parameters obtained from the curve fitting (i.e. adsorption and desorption rates) are listed in Table 1.

Discussion

Interactions between the negatively charged silica surface which is only partially covered with C18 alkyl chains and the dissolved negatively charged albumin molecule present an interesting problem from the point of view of the forces involved. While the electrostatic interactions will induce a long-range repulsion between the surface and the protein molecule, collision of albumin molecules with the surface-immobilized long alkyl chains may result in surface binding due to the short-range hydrophobic interactions. The difference in the distances over which these two forces operate and their opposite signs are expected to create an interesting interaction energy–distance profile: a repulsive energy barrier followed by a steep attractive energy minimum. The height of the barrier can be controlled by the ionic strength of the solution and its effects on protein adsorption should be evident from the adsorption kinetics in the partial C18 coverage region.

In modeling the HSA adsorption, each unit surface area along the C18 surface gradient was assumed to have only two types of protein binding site: C18 and silica. Furthermore, the silica binding sites did not bind albumin; k_{on} for silica was zero. The adsorption saturation, Γ_{max}, at every position along the C18 surface gradient was determined only by the number of C18 binding sites. Figure 5 shows a comparison of the advancing water contact angle, the fractional C18 surface coverage calculated by Eq. (5) and the HSA adsorption profile at the end of the experiment (0.165 M buffer) as a function of the C18 gradient position. The adsorption saturation Γ_{max} was not affected by the number of C18 binding sites when the fractional C18 surface coverage $\Theta/\Theta_{max(C18)} > 0.42$ ($\theta_{adv} > 65°$). At the surface coverage where $\Theta/\Theta_{max(C18)} = 0.42$, the average distance between the C18 chains was approximately 1 nm, so that a globular molecule of the size of albumin could cover roughly 16–25 C18 chains. The average adsorption of HSA, $\Gamma_{hydrophobic}$, measured for a 1 cm length of the fully hydrophobic C18 surface amounted to 0.249 ± 0.014 μg cm^{-2}.

In modeling the adsorption kinetics, only two events were allowed: adsorption and desorption from the surface site. Each process is characterized by the respective rates k_{on} and k_{off}. The modeling of protein adsorption started with the desorption segment of the experiment. Table 1 shows that the initial desorption rates in 0.165 M PBS followed the order $k_{-1(p3)} > k_{-1(p1)} > k_{-1(p2)}$. The initial desorption rates (k_{-1}, Table 1) for the positions p1 and p2 were quite similar: 0.000 51 s^{-1} and 0.000 46 s^{-1} respectively. The initial desorption rate at lower C18 surface coverage (p3; $\Theta/\Theta_{max(C18)} = 0.26$; $\theta_{adv} = 50°$) was higher, $k_1 = 0.000\ 82\ s^{-1}$, indicating that the neighboring negative charges on the silica surface around the C18 surface binding site facilitate the protein's spontaneous desorption. The respective desorption half-lifetimes were 22.7 min, 25 min and 14.1 min. The desorption half-lifetimes in 0.025 M PBS were even shorter, ranging from 6.8 to 8.3 min for different positions along the C18 gradient (Table 1). The difference between the desorption rates in 0.025 M buffer was small (within ± 10% of their average). However, the desorption rates followed the opposite trend, namely $k_{-1(p1)} > k_{-1(p2)} > k_{-1(p3)}$. The 0.025 M buffer does not screen efficiently enough the electrostatic interaction between negatively charged adsorbed proteins. As more adsorbed protein molecules become packed closer to each other, each molecule influences its neighbors through this unscreened repulsive potential. One can hypothesize that the increase in the adsorbed amount causes a faster desorption owing to an increased lateral repulsion between adsorbed HSA molecules.

The initial adsorption rate $k_{1(p1)}$ in 0.165 M PBS ($k_{1(p1)} = 2.0 \times 10^{-2}$ cm^3 μg^{-1} s^{-1}, Table 1) was the highest rate obtained by the fitting procedure for the FITC-HSA concentration used in this study, $c_{HSA} = 42$ μg cm^{-3}. One recalls that at position p1 in 0.165 M PBS the model can only predict the lower limit for k_1 owing to the assumption that the initial adsorption rate at this position is transport limited, i.e. adsorption could proceed faster if there was more protein supplied to the surface. However, this lower limit for $k_{1(p1)}$ is still higher by one order of magnitude than the respective $k_{1(p1)}$ value in 0.025 M PBS ($k_{1(p1)} = 2.5 \times 10^{-3}$ cm^3 μg^{-1} s^{-1}, Table 1). Since the adsorption at the same position p1 from the two buffers of different ionic strength resulted in a similar adsorption saturation, Γ_{max} (0.288 vs. 0.267 μg cm^{-2}), one can conclude that the kinetics of protein binding to the partially covered C18 surface is affected by the different height of the adsorption energy barrier. At the p1

position, $\theta_{adv} = 75°$ and $\Theta/\Theta_{max(C18)} = 0.54$ (Table 1) so that half of the surface is negatively charged silica, giving rise to the adsorption energy barrier. In the buffer solution of higher ionic strength the long-range electrostatic interactions are largely screened, decreasing the height of the adsorption energy barrier and allowing for a faster adsorption. Owing to the low protein solution concentration and the small flow rates, the adsorption was limited by the transport of albumin molecules to the surface. In this case the adsorption rate slows down only when the number of available surface sites becomes limited. A good fit of the experiment to the model required a cooperativity constant α to be equal to two, thus indicating a small effect of negative cooperativity in albumin adsorption.

In the buffer of lower ionic strength the long-range electrostatic interactions are not screened and protein and surface electrostatic potentials start to overlap with each other at larger distances. The increased adsorption energy barrier causes the retardation of the initial adsorption rate; the adsorption is not limited by the transport of molecules to the surface any more. The supply of protein to the surface is high enough and the actual process of adsorption becomes the rate-limiting step. As a result, the adsorption changes from being a transport-limited process to being an adsorption-limited process. The initial adsorption rate decreases by an order of magnitude in 0.025 M PBS: $k_{1(p1)} = 2.4 \times 10^{-3}$ cm^3 μg^{-1} s^{-1}. Interestingly, k_1 in 0.025 M PBS does not change very much with the change in the surface density of the C18 chain. The overwhelming influence of the adsorption energy barrier in 0.025 M PBS largely outweights the subtle balance between the long-range repulsion and the short-range attraction in protein binding. Even at the low C18 surface coverage (p3; $\Theta/\Theta_{max(C18)} = 0.26$; $\theta_{adv} = 50°$), k_1 decreases only by 20% to 1.9×10^{-3} cm^3 μg^{-1} s^{-1}. In comparison, in the case of the screened long-range repulsion in 0.165 M PBS, k_1 drops by 65% between the positions p1 and p3.

It is possible to control the effects of the long-range repulsion and the short-range attraction by controlling the ionic strength in the system. Reverse-phase chromatography depends on these opposing effects. As demonstrated in this study, relatively small differences in the surface density of the hydrophobic ligands are capable of producing significant differences in protein adsorption and desorption. Different brands of the hydrophobic chromatographic supports rarely produce identical separations when run under otherwise identical conditions, probably owing to the small differences in the surface ligand coverage.

The apparent affinity of albumin for the C-18 surface can be estimated from the ratio of the initial adsorption and desorption rates, k_1/k_{-1}, (in M^{-1} units, Table 1). The apparent affinity is plotted in a semilogarithmic plot as a function of C18 surface coverage in Fig. 6. Because of the transport-limited rate at the highest C18 surface coverage, the k_1/k_{-1} value is only the lower limit of apparent affinity (marked with an arrow). In 0.165 M PBS, k_1/k_{-1} decreases more rapidly as the C18 surface coverage $\Theta/\Theta_{max(C18)}$ approaches low values. The apparent affinity in 0.025 M PBS remains unchanged at approximately 1×10^8 M^{-1} across the C18 surface gradient. The fluorescence signal-to-noise ratio made the comparison between the experimental adsorption results at very low C18 surface coverage and the model simulations uncertain.

Jennissen has studied the effect of the surface density of agarose-bound ligands on protein adsorption [35]. The agarose matrices show, in general, very low non-specific protein adsorption. Under the experimental conditions used in the present study, the silica surface was also inert toward albumin adsorption. The adsorption saturation, Γ_{max}, was influenced by the number of C18 binding sites only if the fractional C18 surface coverage $\Theta/\Theta_{max(C18)}$ is less than 0.42 ($\theta_{adv} < 65°$). At this surface coverage the average distance between the C18 chains becomes larger than 1 nm. However, it is uncertain whether the actual distances are equal to the average. The actual distances may be as small as 0.4 nm, which is similar to the densely packed C18 monolayer. If the latter is true, such a dense C18 packing is probably limited to areas of small size with uncovered silica areas in between. If the hypothetical C18 "islands" in the gradient region were much larger than the size of the albumin molecule, the apparent affinity constants should be affected by the average C18 surface coverage and only the adsorption saturation, Γ_{max}, should change. The apparent affinity constants derived for the adsorption experiments in 0.165 M PBS decreased monotonically with the decrease in the C18 surface coverage (Fig. 6). We deduce that the surface distribution of the C18 chains is either random or the C18 "islands" are not much larger than the protein itself. In this case the increase in C18 surface density results in different proportions of the attractive and repulsive protein–surface interactions. By increasing the C18 surface density the electrostatic interactions are proportionally diminished and the apparent affinity constant increased. In 0.025 M buffer, the long-range electrostatic interactions dominate and the effect of the C18 surface density is negligible.

At this point, it is rather difficult to estimate how small the C18 islands are. Atomic force microscopy of mica partially covered with a C18 film showed that the C18 layer grows by nucleating isolated self-similar 90 nm domains [36]. Similar experiments on silica surfaces are now in progress in our laboratory.

Conclusions

The C18 surface density gradient on silica was prepared and used as the liganded adsorbing surface for the FITC-HSA adsorption. The water contact angles showed that the maximal fractional surface coverage of the C18 chains was 0.92. The coverage decreased smoothly to zero in the 12.5 mm long gradient region. FITC-HSA did not adsorb onto the silica end of the gradient surface but adsorbed progressively more onto the surfaces with higher hydrophobicity. The adsorption saturation of FITC-HSA leveled off when the average fractional surface coverage of the C18 chains was larger than 0.42. The adsorption kinetics of FITC-HSA were shown to be influenced by the long-range repulsive electrostatic force, which depended on the ionic strength of the solution from which the adsorption took place, and the short-range hydrophobic interactions. The surface coverage of C18 chains influenced both types of interactions. The adsorption changed from a purely transport-limited process to an adsorption-limited process as the C18 surface coverage decreased. The kinetics of FITC-HSA adsorption were modeled as a simple process with a single forward and reverse rate, including the convective–diffusive transport of protein to the surface. A lower ionic strength of buffer solution decreased the adsorption rates and increased the desorption rates along the C18 gradient. The apparent affinity constant, derived from the adsorption/desorption rates, depended more strongly on the C18 surface coverage in the

0.165 M buffer than in the 0.025 M buffer. The affinity constants indicated that the C18 distribution in the gradient region is either random or that the densely packed C18 islands are not much larger than the protein.

Acknowledgments

Financial support for Y.S. Lin from the Center for Biopolymers at Interfaces, University of Utah, is gratefully acknowledged. We thank Professor H.P. Jennissen for his suggestions and discussions. This research has been partially supported by the NIH research grant RO1 HL44538, a Whitaker Foundation grant to V.H. and the EC research contract #CI1*CT91-0888(LNBE).

References

1. Sevastianov VI. Crit. Rev. Biocompat. 1988; 4:109.
2. Munro MS, Eberhart RC, Maki NJ, Brink BE, Fry WJ. Am. Soc. Artif. Intern. Organs J. 1983; 6:65.
3. Keogh JR, Velander FF, Eaton JW. J. Biomed. Mater. Res. 1992; 26:441. [PubMed: 1376325]
4. Eberhart RC, Munro MS, Frautschi JR, Lubin M, Clubb FJ Jr, Miller CW, Sevastianov VI. Ann. N.Y. Acad. Sci. 1987; 516:78. [PubMed: 3326491]
5. Pitt WG, Grasel TG, Cooper SL. Biomaterials. 1988; 9:36. [PubMed: 3349120]
6. Spector AA. J. Lipid Res. 1915; 16:165. [PubMed: 236351]
7. Goodman DS. J. Am. Chem. Soc. 1958; 80:3892.
8. Van Dulm P, Norde W. J. Colloid Interface Sci. 1983; 91:248.
9. Baszkin A, Lyman DJ. J. Biomed. Mater. Res. 1980; 14:393. [PubMed: 6156944]
10. Gölander CG, Lin YS, Hlady V, Andrade JD. Colloids Surfaces. 1990; 49:289.
11. Grushka, E., editor. Bonded Stationary Phases in Chromatography. Ann Arbor, MI: Ann Arbor Science; 1974.
12. Carr JW, Harris JM. Anal. Chem. 1986; 58:626.
13. Rangnekar VM, Foley JT, Oldham PB. Appl. Spectrosc. 1992; 46:827.
14. Gay JD. J. Phys. Chem. 1974; 78:38.
15. Zeigler RC, Maciel GE. J. Am. Chem. Soc. 1991; 133:6349.
16. Fenter P, Eisenberger P, Li J, Camillone N III, Bernasek S, Scoles G, Ramanarayanan TA, Liang KS. Langmuir. 1991; 7:2013.
17. Schunk TC, Burke MF. Int. J. Environ. Anal. Chem. 1986; 25:81.
18. Morel D, Serpinet J. J. Chromatogr. 1982; 248:231.
19. Tillman N, Ulman A, Schildkraut JS, Penner TL. J. Am. Chem. Soc. 1988; 110:6136. [PubMed: 22148791]
20. Maoz R, Sagiv J. J. Colloid Interface Sci. 1984; 100:465.
21. Ulman, A. An Introduction to Ultrathin Organic Films. Boston, MA: Academic Press; 1991. p. 259
22. Elwing H, Nilsson B, Svensson K-E, Askendahl A, Nilsson UR, Lundstrom I. J. Colloid Interface Sci. 1988; 125:139.
23. Gölander CG, Caldwell K, Lin YS. Colloids Surfaces. 1989; 42:165.
24. Corsel JW, Willems GM, Kop JMM, Cuypers PA, Hermens WTh. J. Colloid Interface Sci. 1986; 111:544.
25. Horsley, DG. M.Sc. Thesis. Salt Lake City, UT: University of Utah; 1988.
26. Kinkel JN, Unger KK. J. Chromatogr. 1984; 316:193.
27. Sander LC, Wise SA. Anal. Chem. 1984; 56:504.
28. Danielson ND, Kirkland JJ. Anal. Chem. 1987; 59:2501.
29. Hlady V. Appl. Spectrosc. 1991; 45:246.
30. Lok BK, Cheng Y-L, Robertson CR. J. Colloid Interface Sci. 1983; 91:87.
31. Lok BK, Cheng Y-L, Robertson CR. J. Colloid Interface Sci. 1983; 91:104.

32. Cuypers PA, Willems GM, Herker HC, Hermens WTh. Ann. N.Y. Acad. Sci. 1987; 516:244. [PubMed: 3439729]
33. Ulman A. J. Mat. Ed. 1989; 11:205.
34. Cassie ABD. Discuss. Faraday Soc. 1952; 75:5041.
35. Jennissen HP. J. Colloid Interface Sci. 1986; 111:570.
36. Schwartz DK, Steinberg S, Israelachvili J, Zasadzinski JAN. Phys. Rev. Lett. 1992; 69:3354. [PubMed: 10046797]

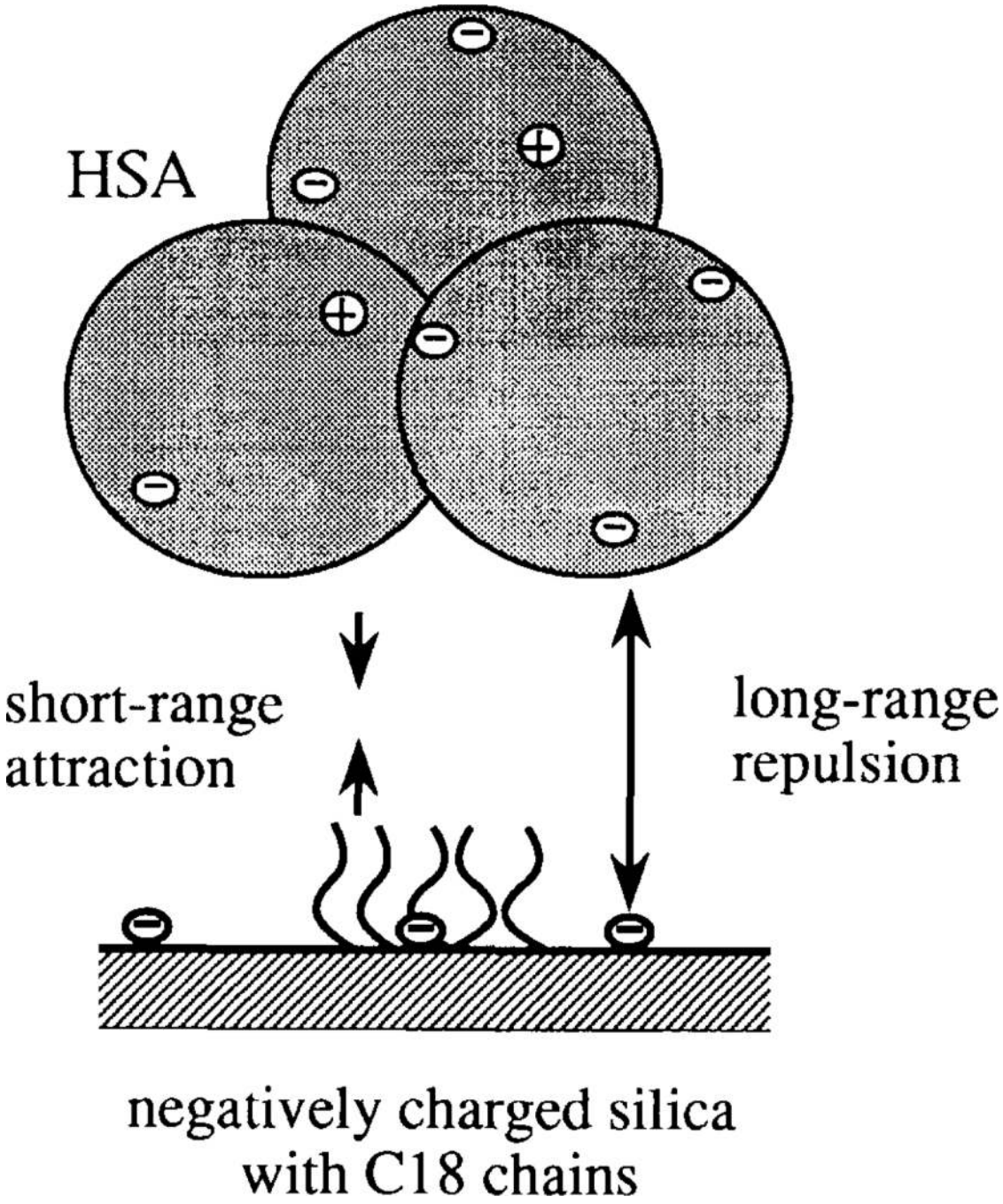

Fig. 1.

A cartoon of the HSA molecule as it approaches the C18–silica surface. The molecule is exposed to a long-range electrostatic repulsion and, when it collides with the C18 surface, to a short-range hydrophobic attraction. The electrostatic repulsion arises from the negatively charged HSA and from negative charges on the silica and/or charged silanol groups that may exist on the silica surface in the C18 layer. The hydrophobic interactions involve the C18 chains on silica and the hydrophobic binding sites on HSA.

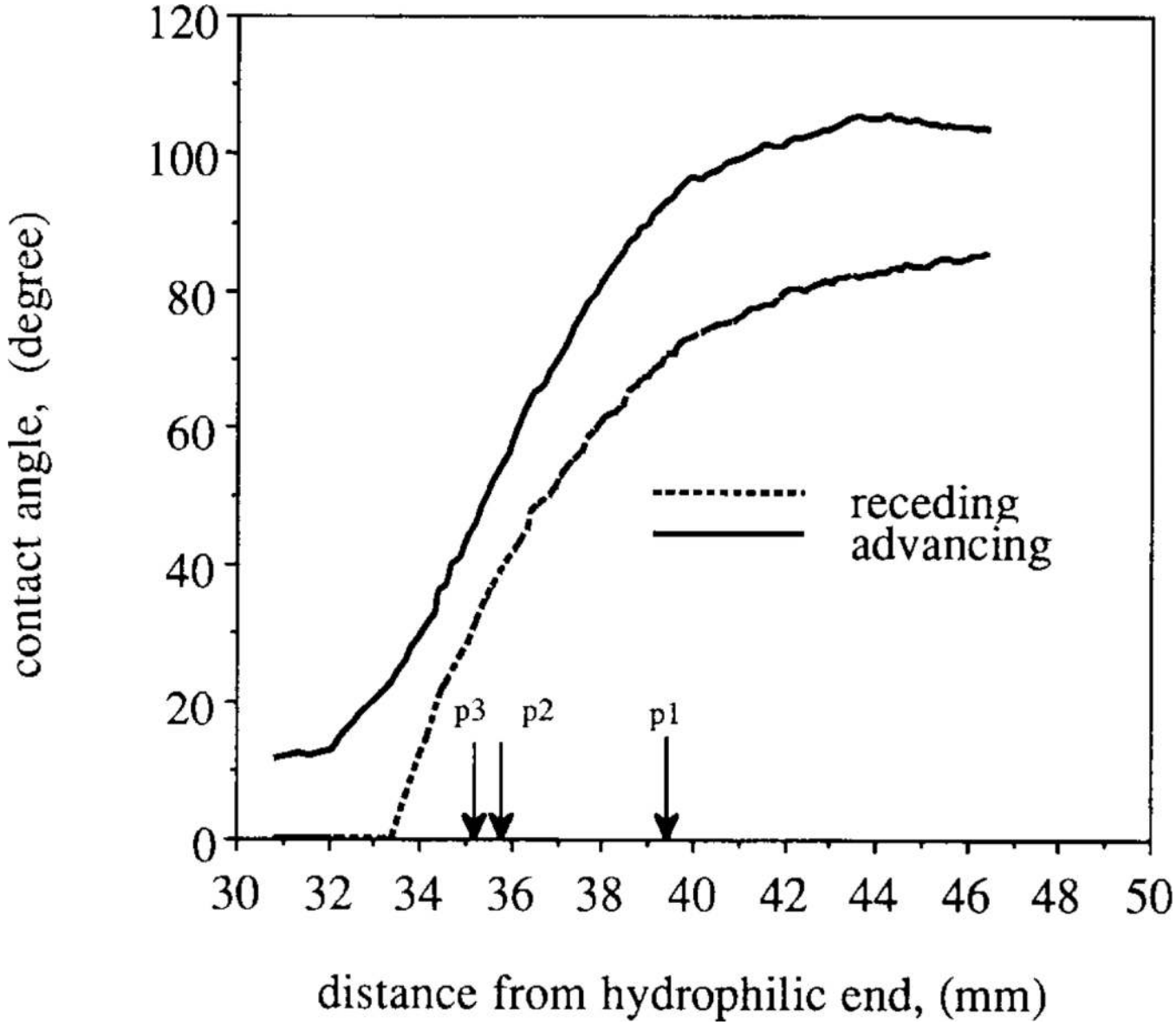

Fig. 2.

The dynamic water contact angle of the octadecyldimethylsilyl (C18)–silica surface density gradient. On the very right-hand side of the gradient is the C18 self-assembled film showing $\theta_{adv} = 105°$ and $\theta_{rec} = 84°$. On the very left-hand side is the silica surface, showing $\theta_{adv} = 12°$ and $\theta_{rec} = 0°$. Arrows labeled p1, p2 and p3 indicate the positions at which the experimental adsorption results were fitted to the model described by Eq. (2).

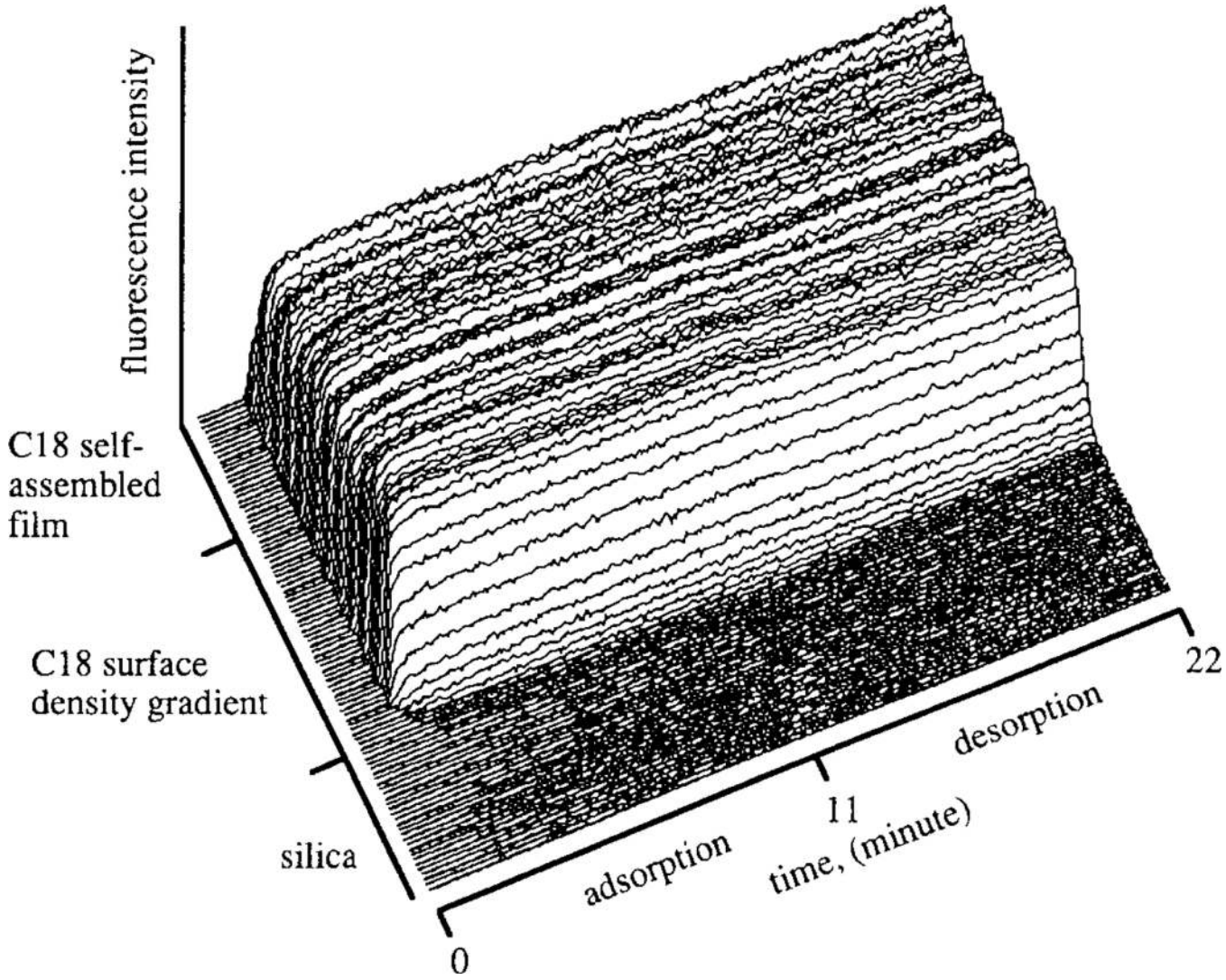

Fig. 3.

The TIRF pattern for the FITC-HSA adsorption/desorption experiment. The HSA adsorption took place from the flowing FITC-HSA solution (c_{HSA} = 42 μg ml^{-1} in PBS; pH 7.4; 0.165 M ionic strength) for 11 min. The experiment was continued by the desorption segment during which only the buffer solution (PBS; pH 7.4; 0.165 M ionic strength) flowed through the TIRF cell for an additional 11 min. The flow rates were 1 ml min^{-1}. The vertical axis is the fluorescence intensity of surface-bound FITC-HSA. During each TIRF experiment the fluorescence intensity was simultaneously measured along the C18 surface gradient every second and combined into an intensity–time–space data array shown here. The experimental procedure and the accompanying technical details of the spatially resolved TIRF technique can be found in Ref. 29.

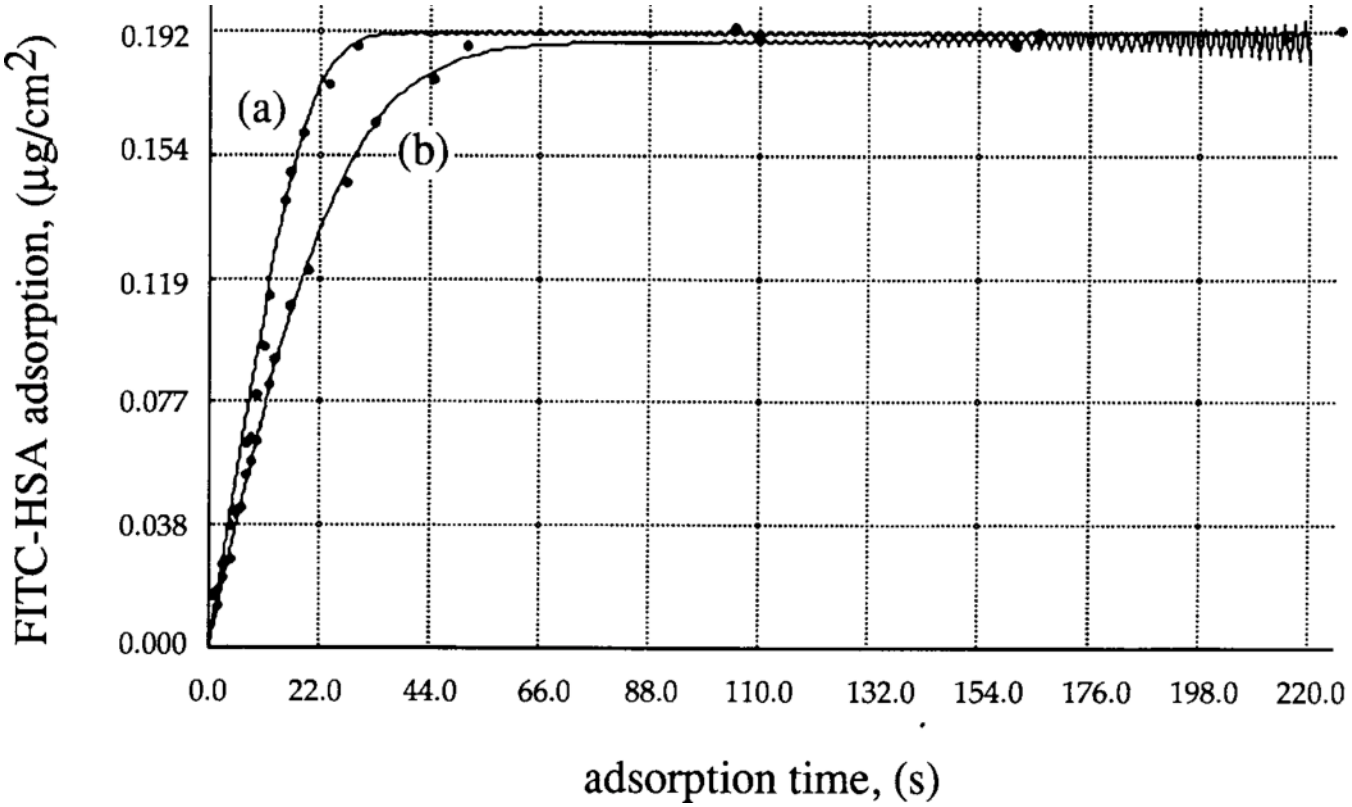

Fig. 4.

Comparison between the experimental FITC-HSA adsorption onto the p2 position of the C18 surface gradient (p2; $\theta_{adv} = 54°$; $\Theta/\Theta_{max(C18)} = 0.30$) (filled circles) and HSA adsorption model (solid lines). The data for the two buffer solutions of low and high ionic strength, 0.025 M and 0.165 M, are shown. The modeling parameters used to produce a fit shown here are listed in Table 1.

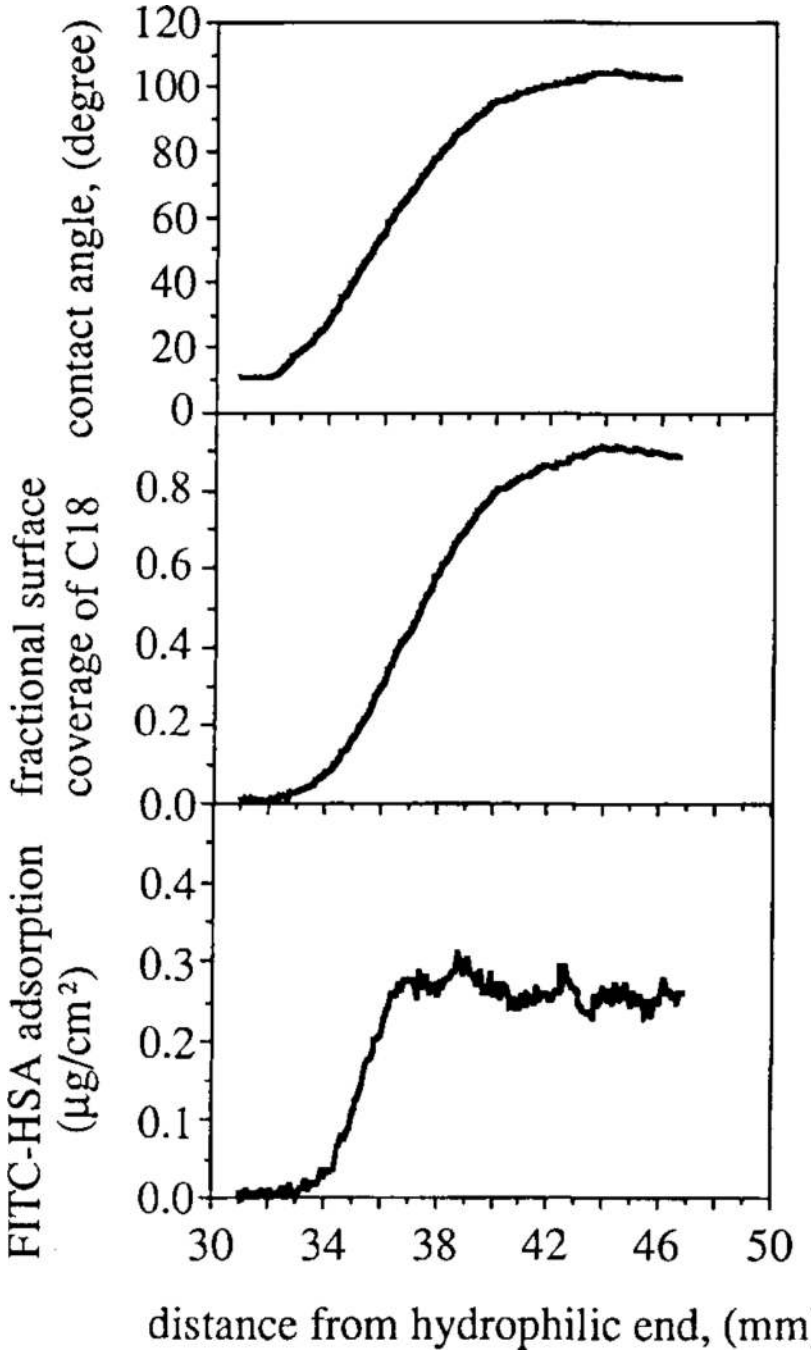

Fig. 5.

Comparison of the advancing water contact angle, the fractional C18 surface coverage and the HSA adsorption profile (0.165 M buffer) as a function of the C18 gradient position.

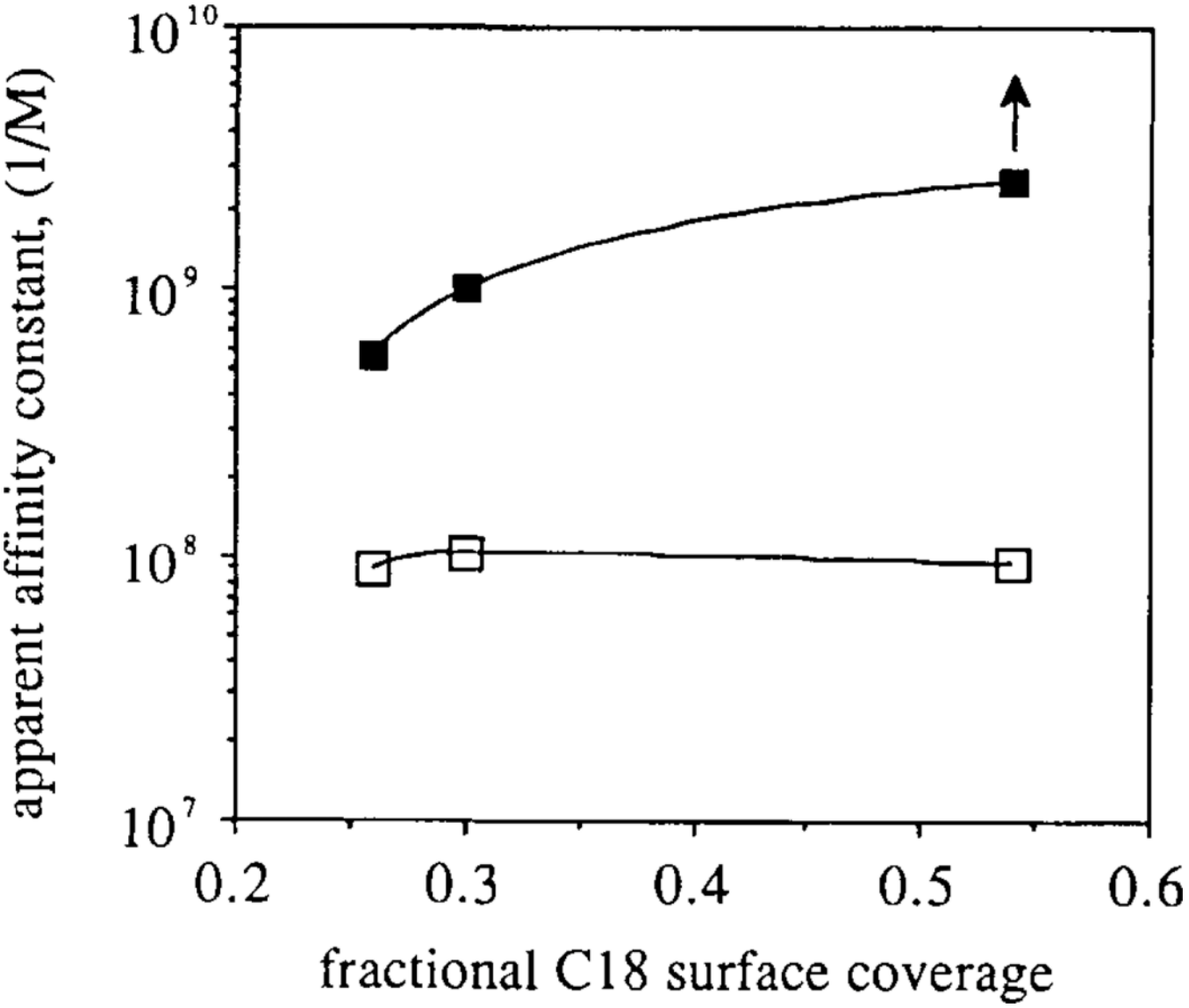

Fig. 6.

The apparent affinity constant of FITC-HSA binding to the C18 surface, k_1/k_{-1} (M^{-1}) shown as a function of the fractional C18 surface coverage. The arrow indicates that only the lower limit of apparent affinity could be calculated: □, solution ionic strength 0.025 M; ■, solution ionic strength 0.165 M.

Table 1

The α, β, k_1 and k_{-1} values used in the fitting of the first 5 min of HSA adsorption at the pl, p2 and p3 positions[a] (see Fig. 2) to the model described by Eq. (2)

Parameter	θ_{adv}, position					
	75°, p1	**54°, p2**	**50°, p3**	**75°, p1**	**54°, p2**	**50°, p3**
α	2	0	2	0	0	0
β	0	0	0	0	0	0
k_1 ($cm^3\ \mu g^{-1}\ s^{-1}$)	$>2.0 \times 10^{-2}$	7×10^{-3}	7×10^{-3}	2.4×10^{-3}	2.4×10^{-4}	1.9×10^{-3}
k_{-1} (s^{-1})	5.1×10^{-4}	4.6×10^{-4}	8.2×10^{-4}	1.71×10^{-3}	1.55×10^{-3}	1.40×10^{-3}
k_1/k_{-1}[b] (M^{-1})	$>2.59 \times 10^9$	1.00×10^9	5.63×10^8	9.26×10^7	1.02×10^8	8.96×10^7
ln $2/k_{-1}$[c] (min)	22.7	25.1	14.1	6.8	7.5	8.3
Ionic strength (M)	0.165	0.165	0.165	0.025	0.025	0.025
$\Theta/\Theta_{max(C18)}$[d]	0.54	0.30	0.26	0.54	0.30	0.26
$\Gamma_{max(FITC\text{-}HSA)}$[e] (μg cm^{-2})	0.288	0.192	0.146	0.267	0.198	0.163

[a] The water contact angles were $\theta_{adv} = 75°$ and $\theta_{rec} = 55°$ for position p1, $\theta_{adv} = 54°$ and $\theta_{rec} = 39°$ for position p2, and $\theta_{adv} = 50°$ and $\theta_{rec} = 35°$ for position p3.

[b] Apparent affinity constant.

[c] Desorption half-lifetime.

[d] C18 surface coverage calculated by the Cassie equation (Eq. (1)) from the respective θ_{adv} values.

[e] Adsorption saturation of HSA.